Signal Process. Renew. Energy., 2026; 10(1): 34-48

Signal Processing and Renewable Energy (SPRE)

https://doi.org/10.57647/spre.2026.1001.04

Research Article

Robust Control of Proton Exchange Membrane Fuel Cell Equipped by Boost Converter

Hasan Khosh Kholgh Sima, Alireza Sahab*, Abdolreza Tavakli, Hossein MahdiNia

Department of Electrical Engineering, La.C., Islamic Azad University, Lahijan, Iran

***Corresponding author:** Alireza.Sahab@iau.ac.ir

Article History:

Received:
3 June 2025

Revised:
22 December 2025

Accepted:
19 February 2026

Published in Issue:
31 March 2026

Abstract

Given the critical role of energy in modern life, this article introduces a novel approach to enhance and optimize the power output of PEM fuel cells. The study focuses on a PEM fuel cell system equipped with a boost converter and proposes a robust hybrid control strategy for the boost converter to maximize power extraction from the PEM fuel cell source. The proposed hybrid robust method combines two well-known techniques. The first is the reset control technique, which, despite its simplicity, excels in eliminating regulatory errors, improving transient and steady-state responses, and overcoming the limitations of linear controllers. The second is the sliding mode control (SMC) technique, specifically the Adaptive Super-Twisting Sliding Mode Control. This method ensures robustness and fast controller performance against uncertainties and disturbances. The proposed control strategy enhances the boost converter's efficiency, thereby increasing the power extracted from the PEM fuel cell. Additionally, it stabilizes the output voltage of the PEM fuel cell, achieving higher power output compared to alternative methods. Implementation results in the MATLAB environment, along with comparisons to the adaptive sliding mode-PI method, confirm the effectiveness and superiority of the proposed robust hybrid approach.

Keywords: Fuel cell; PEM fuel cell; Boost converter; Reset control; Adaptive super twisting sliding mode control; Uncertainty; Lyapunov; Output power

Cite this article: Khosh Kholgh Sima, H., Sahab, A., Tavakli, A., MahdiNia, H., Robust Control of Proton Exchange Membrane Fuel Cell Equipped by Boost Converter, *Signal Process. Renew. Energy. 10*(1) 34-48 (2026). https://doi.org/10.57647/spre.2026.1001.04

1. Introduction

In recent years, the development and utilization of renewable energy sources have grown significantly. The primary reasons for this growth include the intermittent nature of renewable energy resources, the rapid depletion of fossil fuel reserves, and the rising global demand for energy [1-2]. Additionally, advancements in technology and increased investments have accelerated the transition toward renewable energy sources. Among the most prominent renewable energy resources discussed in this study are hydrogen fuel cells. Hydrogen energy and fuel cells are considered among the most promising alternatives for green and sustainable energy in the future. Depending on whether hydrogen is produced from renewable or non-renewable primary

energy sources, it results in either minimal or zero carbon emissions and pollution. Furthermore, hydrogen fuel cells are more efficient in energy conversion compared to other renewable energy technologies [3].

Among fuel cell types, Proton Exchange Membrane Fuel Cells (PEMFCs) offer several advantages, including a short startup time, high power density, and relatively low operating temperatures. These characteristics make PEMFCs highly suitable for a variety of applications, such as stationary power generation, portable energy devices, and electric vehicles, where clean and efficient energy conversion is essential [4].

Due to their numerous operational and environmental benefits, PEMFCs are pivotal in the clean energy domain and for achieving sustainable transportation. PEMFCs are zero-emission energy sources that do not produce SOX, NOX, or CO2. Electricity is generated via an electrochemical reaction, with water being the only byproduct [5]. This starkly contrasts with traditional combustion engines, which emit greenhouse gases and air pollutants contributing to climate change and poor air quality.

Key Benefits of PEMFCs are:

1. High Energy Conversion Efficiency: PEMFCs have a higher energy conversion efficiency compared to internal combustion engines, as they directly convert chemical energy into electricity without intermediate heat generation stages. This reduces energy losses and improves fuel utilization, contributing to sustainability.
2. Renewable Hydrogen: Hydrogen used in PEMFCs can be produced from renewable energy sources, such as solar, wind, and hydropower, through water electrolysis. This makes hydrogen a sustainable and renewable energy carrier suitable for clean power generation in PEMFCs.
3. Decarbonization of Transportation: Using PEMFCs in electric vehicles (EVs) can significantly reduce carbon emissions in the transportation sector, a major contributor to greenhouse gas emissions. Fuel cell electric vehicles (FCEVs) are particularly advantageous for long-range transportation and heavy-duty vehicles due to their extended driving range and faster refueling times compared to battery electric vehicles (BEVs).
4. Grid Stability and Energy Storage: PEMFCs, especially when integrated with renewable energy sources, can enhance grid stability by providing distributed power generation and energy storage solutions. They store excess electricity generated during periods of low demand and supply it back to the grid during peak demand, fostering a more resilient energy infrastructure.

While PEMFCs hold immense potential for clean energy and eco-friendly transportation, challenges related to cost, performance, and durability remain barriers to their widespread adoption. PEMFCs operate as electrochemical energy conversion devices, generating electricity from the chemical reaction between hydrogen and oxygen. These cells consist of an anode, a cathode, and a proton exchange membrane sandwiched between them. Initially, fuel cells were developed as single cells but were later adapted into stack configurations to adjust power ratings based on connected loads.

A PEMFC stack configuration is illustrated in figure 1, showcasing its design for scaling up power output efficiently to meet varying energy demands.

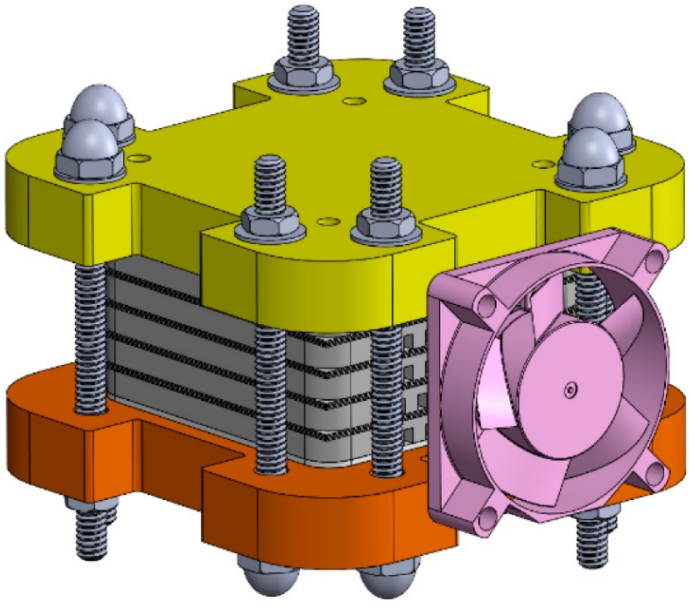

Figure 1. A PEMFC stack configuration

10.57647/spre.2026.1001.04

Performance, cost, and durability remain the three primary challenges that PEMFC technology must overcome for widespread adoption and successful application in various fields. From a performance perspective, factors such as the conductivity of the proton exchange membrane, the catalytic efficiency of electrochemical reactions, and mass transport within the fuel cell significantly impact the efficiency and power density of PEMFCs. Addressing these areas is essential for improving their performance.

While the aforementioned challenges largely pertain to the structural and design modifications of PEM fuel cells, post-construction theoretical approaches must also be considered more extensively. One notable area of study involves integrating PEM fuel cell structures with power electronics, a topic that has been explored through valuable and relatively comprehensive research. Building on these efforts, this paper aims to maximize the power extraction from PEM fuel cells by implementing a novel robust control strategy on the boost converter located at the fuel cell stack's output. The studied structure ensures a stabilized output voltage level while enabling optimized power output. To further enhance stack performance, this research proposes a hybrid robust control method that emphasizes theoretical post-construction strategies for maximizing power extraction.

One of the most common configurations for converting PEM fuel cell output power involves DC/DC converters. Various topologies are available for DC/DC converters, including buck converters (voltage reduction), boost converters (voltage elevation), and combined buck-boost converters [6]. These converters utilize Pulse Width Modulation (PWM) switching techniques to regulate the DC output voltage. To achieve higher efficiency in power conversion from the fuel cell stack to the load, numerous control techniques have been employed to ensure the system operates at its maximum power point. However, the nonlinearity of the system, coupled with uncertainties and disturbances, renders classical linear control methods for DC/DC converters ineffective.

Recently, advanced techniques such as Artificial Neural Networks (ANN), Particle Swarm Optimization (PSO), feedback linearization [7], Fuzzy Logic Controllers (FLC) [8, 9], and Sliding Mode Controllers (SMC) [10–13] have gained widespread attention in the literature. Among these, the Sliding Mode Controller (SMC) is frequently used due to its numerous advantages, including system stabilization against parameter variations and load disturbances [14–16], ease of implementation, and robust performance in diverse applications [17–18].

Despite its strengths, the implementation of SMC in DC/DC converters presents several significant challenges:

1. Variable Switching Frequency: This generates low-frequency harmonic components, complicating the filtering process.
2. Steady-State Error: Although SMC offers robustness against parameter variations and disturbances, a non-zero steady-state error is observed.
3. System Instability: Many DC-DC converters designed to improve the power output of PEM fuel cells, such as PI + ASM-controlled boost converters, are non-minimum phase systems. The presence of a right-half-plane zero in the transfer function of the DC-DC boost converter causes direct voltage control to destabilize the overall system.
4. Neglected Parasitic Effects: Certain parasitic and detrimental effects, such as voltage drops across the power switch, semiconductor diode, and equivalent series resistance of the output capacitor, are often omitted from the dynamic and static equations governing converter behavior. These factors make it impractical to treat model parameters as constants.

To address these issues and maximize the power output from PEM fuel cells, this paper introduces an indirect robust voltage control method. The planned approach is based on a hybrid Proportional-Integral (PI) and Adaptive Sliding Mode (ASM) control technique. This method stabilizes the PEM fuel cell system across its entire operational range while accounting for parameter uncertainties.

- Proportional-Integral (PI) Method: This is employed to eliminate steady-state error.
- Sliding Mode Control (SMC): Used for output voltage regulation and stabilization under load variations and parameter changes.
- Adaptive Mechanism: Designed to estimate and handle high uncertainty bounds within the system.

The remainder of the paper is organized as follows:

Section 2 presents the PEM fuel cell model integrated with the DC-DC converter. Section 3 describes the structure of the proposed control strategy. Section 4 provides simulation results and comparisons conducted in the MATLAB environment. Section 5 concludes the study with insights and suggestions for future work.

2. Model of PEM Fuel Cell Stack with Boost Converter

This section outlines the dynamic model of a Proton Exchange Membrane Fuel Cell (PEMFC) system integrated with a DC/DC boost converter.

10.57647/spre.2026.1001.04

The primary role of the PEM fuel cell is to transform chemical energy into electrical energy through oxidation, reduction, and combination reactions occurring in various parts of the fuel cell. The schematic representation of the main components of a PEM fuel cell, as depicted in figure 2, includes three primary parts: the anode, cathode, and membrane.

During the chemical reactions within the fuel cell, electrical energy is generated along with a significant amount of water as a byproduct. Additionally, the output voltage of a single cell and the fuel cell stack can be mathematically expressed through the following equations [19,20]:

$$V_{Fc} = E_{Cell} - \eta_{act} - \eta_{ohm} - \eta_{con} \quad (1)$$

$$V_{stack} = N_{cell}.V_{Fc} = N_{cell}.(E_{cell} - \eta_{act} - \eta_{ohm} - \eta_{con}) \quad (2)$$

In Equations (1) and (2):

- E_{Cell} represents the electrochemical thermodynamic potential of the PEMFC, signifying the ideal voltage output.

-η_{act} accounts for activation polarization loss, which arises due to the activation energy required at the anode and cathode.

- η_{ohm}represents ohmic polarization loss, which is caused by the resistance of the membrane to proton movement and the electrode resistance to electron flow.

- η_{con} refers to concentration polarization loss, resulting from the reduced concentration of reactants (oxygen and hydrogen) at the reaction sites.

- $N_{cell}$is the number of cells in the fuel cell stack.

These equations capture the key losses associated with PEMFC operation, helping to understand the deviation from the ideal voltage and highlighting the significance of optimizing these factors for better performance.

Given the similarity of the PEM cell membrane to a capacitor (due to its position between two charged layers), and by applying Kirchhoff's circuit laws along with reference [19], the output voltage of the PEM fuel cell can be further expressed as another equation.

$$V_{cell} = E_{cell} - \left(\frac{R_{act}+R_{con}}{(R_{act}+R_{con})C.s+1} + R_{ohm}\right) I \quad (3)$$

Here, R_{ohm}, R_{act}, and R_{con}correspond to ohmic, activation, and concentration resistances, respectively, while C is the equivalent capacitance. This approach models the dynamic electrical behavior of the PEMFC, reflecting its internal processes and losses during operation.

To achieve a more detailed understanding of PEMFC behavior, partial equations for oxygen and hydrogen dynamics (Equations 4 and 5) are introduced.

$$P_{H_2} = \frac{1/K_{H_2}}{(1+\tau_{H_2})}(q_{H_2} - 2I.K_r) \quad (4)$$

$$P_{O_2} = \frac{1/K_{O_2}}{(1+\tau_{O_2})}(q_{O_2} - I.K_r) \quad (5)$$

where:

$$\begin{cases} \tau_{H_2} = \dfrac{V_{an}}{R.T.K_{H_2}} \\ \tau_{O_2} = \dfrac{V_{an}}{R.T.K_{O_2}} \end{cases} \quad (6)$$

These equations account for critical factors such as:

- K_{H_2}: Valve molar constant for hydrogen (\(kmol/s \cdot atm\)).
- K_{O_2}: Valve molar constant for oxygen (\(kmol/s \cdot atm\)).
- q_{H_2}: Hydrogen flow rate.
- q_{O_2}: Oxygen flow rate.
- τ_{H_2}: Response time of hydrogen (\(s\)).
- τ_{O_2}: Response time of oxygen (\(s\)).
- K_r: Modeling parameter constant (\(kmol/(s \cdot A)\)).
- V_{an}: Volume of the anode.

By incorporating these parameters, the model becomes more representative of real-world fuel cell behavior, capturing dynamic response characteristics of the reactants and their flow rates.

Figure 3 visually depicts the behavior of the PEM fuel cell system, illustrating the interplay of these factors.

After deriving the detailed model of the PEM fuel cell, attention shifts to the dynamic modeling of the DC/DC boost converter. The boost converter's primary role is to step up the input voltage from the PEM fuel cell to a higher output voltage level, as illustrated in figure 4.

The converter comprises the following key components:

1. A DC voltage source (the PEM fuel cell).
2. A transistor switch.
3. An inductor.
4. A diode switch.
5. A filter capacitor.
6. An ohmic load.

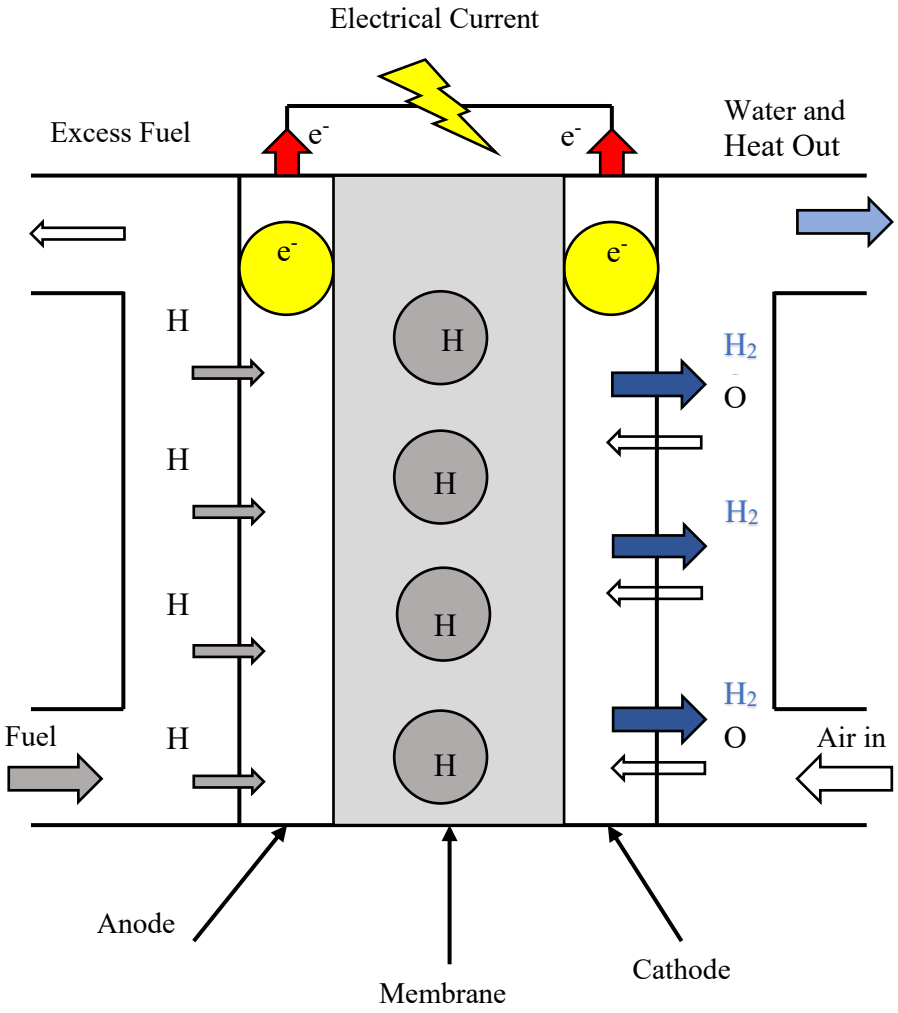

Figure 2. The schematic representation of the main components of a PEM fuel cell

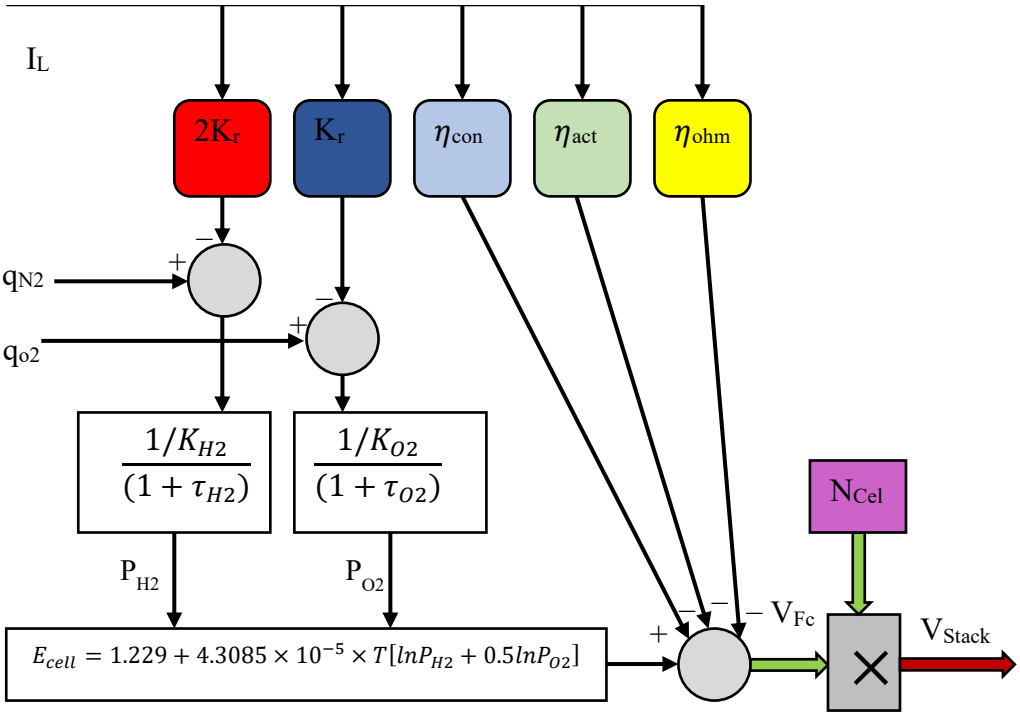

Figure 3. The PEMFC dynamic behavior

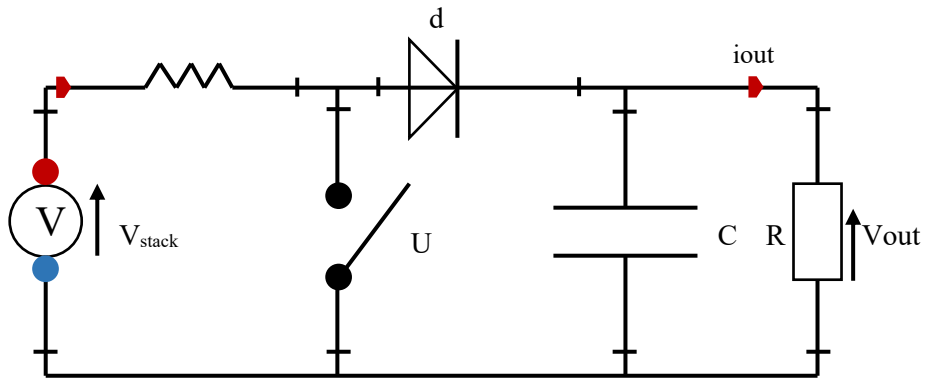

Figure 4. The design of the DC/DC boost converter circuit

The switching mechanism (u) determines the output behavior and governs the operation of the boost converter in two modes:

$$V_{out} = \left(\frac{1}{1-u}\right).V_{stack} \tag{7}$$

1. Mode 1: When the transistor switch (u) is ON and the diode (d) is OFF. In this state, the dynamic equations for the inductor current and output voltage are defined.

$$\begin{cases} \frac{di_L}{dt} = \frac{1}{L}(V_{stack}) \\ \frac{dV_{out}}{dt} = \frac{1}{C}(-i_{out}) \end{cases} \tag{8}$$

2. Mode 2: When the transistor (u) is OFF and the diode (d) is ON. Corresponding dynamic equations are also defined for this state.

These two modes highlight the fundamental operation of the boost converter, emphasizing the importance of accurate switching to maintain voltage regulation.

By substituting the inductor current and output voltage into state variables, along with $V_{stack} = v$, the state-space representation for the boost converter is obtained in Equation (10). This equation forms the foundation for analyzing the dynamic behavior of the boost converter in the PEMFC system.

$$\begin{cases} \frac{di_L}{dt} = \frac{1}{L}(V_{stack} - V_{out}) \\ \frac{dV_{out}}{dt} = \frac{1}{C}(i_L - i_{out}) \end{cases} \tag{9}$$

$$\begin{cases} \dot{x} = \begin{pmatrix} 0 & \frac{u-1}{L} \\ \frac{1-u}{C} & -\frac{1}{RC} \end{pmatrix} x + \begin{bmatrix} \frac{1}{L} \\ 0 \end{bmatrix} v \\ y = [0 \quad 1]x \end{cases} \tag{10}$$

The parameters for the PEM fuel cell are provided in Table 1, offering a comprehensive overview of system specifications. For further details on the model, references [19-22] can be consulted.

3. Proposed Robust Joint Reset Adaptive Super Twisting Sliding Mode Controller

This section outlines a novel control strategy designed to maximize power extraction from a PEM fuel cell system while maintaining a stable output voltage from the stack, which is connected to a boost converter. The proposed hybrid controller integrates two primary approaches: the reset robust technique and the adaptive sliding mode method.

Table 1. The parameters of the PEM fuel cell

Symbol	Value	Unit
E_O	1.229	V
R	83.143	$J\ mol^{-1}K^{-1}$
F	96485.309	$C\ mol^{-1}$
T	298.15	K
A	162	c
ψ	23	
l	175.10^{-6}	cm
B	0.1	V
R_c	0.0003	
J_{max}	0.062	$A\ cm^{-1}$
N_{cell}	10	
ξ_1	0.9514	V
ξ_2	-0.00312	V/K
ξ_3	$-7.4.10^{-5}$	V/K
ξ_4	$1.87.10^{-4}$	V/K

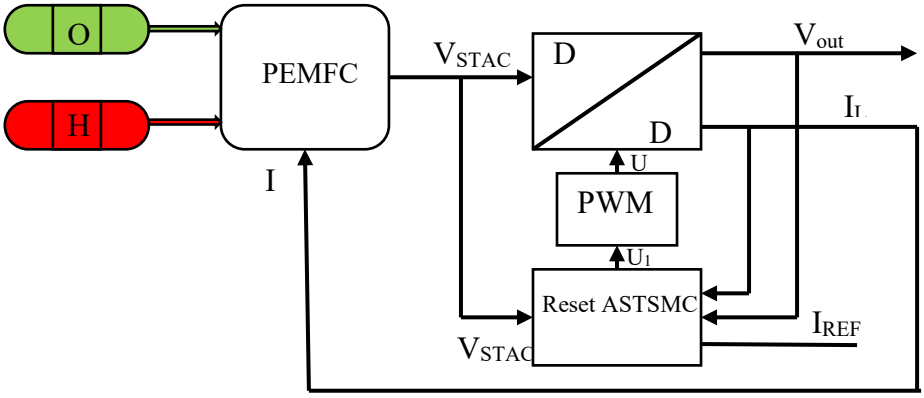

Figure 5. The structure of the planned control approach for the PEMFC stack power system

The reset robust technique is implemented in the inner control loop due to its exceptional ability to eliminate steady-state tracking errors, achieve rapid regulation, and enhance the dynamic response of the closed-loop system. Additionally, it effectively addresses the challenges posed by the non-minimum phase characteristics of the DC/DC boost converter and mitigates the adverse impacts of model uncertainties and input disturbances within the PEM fuel cell system.

The outer loop incorporates the adaptive sliding mode method, a widely recognized robust control approach capable of handling parameter variations and external disturbances. This method, combined with the adaptive framework, ensures reliable performance in environments where the fuel cell system is subjected to significant uncertainties, environmental fluctuations, and external perturbations.

By leveraging the synergy of these techniques, the proposed control approach achieves maximum power extraction from the fuel cell stack while guaranteeing system stability under unknown and varying conditions. Moreover, it ensures zero tracking error for the inductor current. The detailed structure of the controller is illustrated in figure 5.

Considering V_{stack}, i_{ref}, i_L, and V_{out}, the proposed method provides precise control over the boost converter to achieve the desired i_L, and V_{out}. The steps for designing the controller are outlined below.

By incorporating the reset technique, the dynamic behavior of the output voltage can be described as follows:

$$\begin{aligned} V_{ref} &= k_P(x_1 - i_{ref}) \\ &+ k_I \int (x_1 - i_{ref})dt \\ &+ \kappa_{iReset} \int_{Reset} (x_1 - i_{ref})dt \end{aligned} \tag{11}$$

Here, k_P, k_I, and κ_{iReset} represent the controller gains. In continuous conduction mode (CCM), the relationship between the output voltage and the input voltage is given by:

$$V_{out} = \frac{V_{stack}}{1-u} \tag{12}$$

The output current is connected to the input current as follows:

$$I_{out} = (1-u)I_{in} \tag{13}$$

Under ideal conditions and assuming $P_{in} = P_{out}$, the output resistance can be expressed as:

$$R_{out} = \frac{R_{in}}{(1-u)^2} \tag{14}$$

From this, it follows that:

$$R_{in} = (1-u)^2 \tag{15}$$

Analyzing this relationship reveals that an increase in the duty cycle u leads to a decrease in R_{in}. Consequently, based on $P = RI^2$, the input current will increase. This implies that the rate of change of the duty cycle is directly proportional to the rate of change of the current. Mathematically, this can be expressed as:

$$sign(u) = sign(I) \tag{16}$$

The selection of the sliding switching surface is formulated as follows:

$$\begin{aligned} S(x) &= k_P(x_1 - i_{ref}) \\ &+ k_I \int (x_1 - i_{ref})\, dt \\ &+ \kappa_{iReset} \int_{Reset} (x_1 - i_{ref})\, dt \end{aligned} \tag{17}$$

To achieve the control objective using the adaptive sliding mode technique, it is crucial to satisfy the following condition for the sliding surface:

$$\frac{dS}{dt} = 0 \tag{18}$$

Taking Equation (13) into account, Equation (15) transforms into:

$$\begin{aligned}\dot{S} = k_P\left(\tfrac{1}{L}(V - x_2) + \tfrac{1}{L}u\right) \\ +k_I(x_1 - i_{ref}) + \kappa_{iReset}\left(\int_{Reset}(x_1 - i_{ref})dt\right)' \\ = w(x,v,u) + u\end{aligned} \tag{19}$$

Where

$$\begin{aligned}w(x,v,u) = k_I(x_1 - i_{ref}) \\ +\kappa_{iReset}\left(\int_{Reset}(x_1 - i_{ref})dt\right)' \\ +\frac{k_P}{L}(V - x_2) + \frac{k_P - L}{L}u\end{aligned} \tag{20}$$

The Lyapunov method is a robust approach used to ensure system stability and design control strategies that achieve desired goals, even in the presence of uncertainties or disturbances. In this context, a Lyapunov candidate function is chosen, as presented in Equation (21). This function serves as a mathematical tool to evaluate the system's stability.

$$V = |S| + \frac{1}{2\lambda}\widetilde{W}^2 \tag{21}$$

and

$$|w(x,v,u)| < W \tag{22}$$

The parameter λ represents the adaptive rule regulation, which dynamically adjusts the control law to account for changes in system behavior. The term $\widetilde{W}$ denotes the difference (or error) between the actual unknown upper bound W of $w(x,v,u)$ and its estimation $\widehat{W}$. The purpose of estimating this upper bound is to account for uncertainties or disturbances that may arise during operation.

By differentiating the Lyapunov function, a stability criterion is derived, ensuring that the system's state trajectory remains bounded and converges to the desired sliding surface.

$$\dot{V} = \dot{S}sign(S) - \frac{1}{\lambda}\widetilde{W}\dot{\widehat{W}} \tag{23}$$

By replacing, we have

$$\dot{V} = (w(x,v,u) + u)sign(S) - \frac{1}{\lambda}\widetilde{W}\dot{\widehat{W}} \tag{24}$$

This approach not only guarantees stability but also optimizes performance by continuously adapting to the system's conditions. It plays a critical role in achieving precise control, especially in complex systems like PEM fuel cells with boost converters, where uncertainties and non-linearities are significant.

To ensure the stability of the control signal, it is divided into two main components: one for system stability (u_1) and the other for addressing uncertainties through adaptive control (u_2). The combined control signal is expressed as:

$$u = u_1 + u_2 \tag{25}$$

where u_1 ensures the system's stability, and u_2 is responsible for managing the uncertain parts of the system based on adaptive control.

u_1 - System Stability

This component of the control signal is designed using the Super Twisting Sliding Mode method. This approach is highly effective due to its robustness against rapid system changes and external disturbances, providing reliable performance. Moreover, it reduces oscillatory effects and mitigates the issue of high-frequency switching ripple, thereby improving system stability. The control signal u_1 is divided into two parts as follows:

$$u_1 = u_{11} + u_{12} \tag{26}$$

With the dynamics of each part defined as:

$$\dot{u}_{11} = -k_1 sign(S) \tag{27}$$

$$\dot{u}_{12} = -k_2|S|^{0.5}sign(S) \tag{28}$$

u_2 - Managing Uncertainties

The second component, u_2, is based on adaptive control. This method minimizes the effects of uncertainties and parametric variations in the system. By estimating and adjusting the varying parameters of the system, the adaptive control ensures that the effects of uncertainties are effectively reduced. The control signal u_2 is defined as:

$$u_2 = -\widehat{W} \tag{29}$$

These two components work together to not only guarantee the stability of the system but also improve performance in the presence of disturbances and parameter variations. This hybrid control structure

creates a robust and adaptive system capable of maintaining optimal performance under varying operational conditions.

By defining the control input as follows:

$$u = -k_1 \int sign(S)dt - k_2|S|^{0.5}sign(S) - \widehat{W} \quad (30)$$

and substituting Equation (30) into Equation (24), the resulting expression can be formulated as:

$$\dot{V} = \left(w(x,v,u) - k_1 \int sign(S)dt - k_2|S|^{0.5}sign(S) - \widehat{W}\right)sign(S) - \frac{1}{\lambda}\widetilde{W}\dot{\widehat{W}} = -(k_1 t + k_2|S|^{0.5})sign(S)^2 + \left(w(x,v,u) - \widehat{W}\right)sign(S) - \frac{1}{\lambda}\widetilde{W}\dot{\widehat{W}} \quad (31)$$

This step ensures that the control input directly integrates into the system dynamics, establishing the foundation for achieving the desired control objectives. To derive the adaptive rule, we reformulate Equation (31) as:

$$\dot{V} \le -(k_1 t + k_2|S|^{0.5})sign(S)^2 + sign(S)\left(W - \widehat{W}\right) - \frac{1}{\lambda}\widetilde{W}\dot{\widehat{W}} \quad (32)$$

Rewriting this equation allows for a clearer identification of the relationship between the adaptive error $\widetilde{W}$ and its coefficient, ensuring the derivation of a proper adaptive law.

$$\dot{V} \le -(k_1 t + k_2|S|^{0.5})sign(S)^2 + \widetilde{W}\left(sign(S) - \frac{1}{\lambda}\dot{\widehat{W}}\right) \quad (33)$$

From Equation (33), in order to eliminate the adaptive error $\widetilde{W}$, its coefficient must be set to zero. Achieving this requires determining the adaptive rule, which is expressed as follows:

$$\dot{\widehat{W}} = \lambda sign(S) \quad (34)$$

Setting the coefficient of $\widetilde{W}$ to zero is a critical step, as it eliminates the impact of the adaptive error on system performance, ensuring robustness against uncertainties. By substituting Equation (34) into Equation (33), the following result is obtained:

$$\dot{V} \le -(k_1 t + k_2|S|^{0.5})sign(S)^2 \quad (35)$$

The above inequality shows that $\dot{V}$ is negative definite, and this substitution confirms that the adaptive law is correctly integrated into the system, ensuring that the error is minimized effectively.

Equation (35) demonstrates that, through the implementation of the control signal defined in Equation (30) and the adaptive rule derived in Equation (34), the stability of the closed-loop system is guaranteed in the asymptotic stability concept. Additionally, it confirms that the control objectives are effectively achieved. This conclusion highlights the reliability of the proposed control methodology, showing that it can stabilize the system while addressing uncertainties and external disturbances.

In the next section, a simulation in the MATLAB software environment will be used to show the controller's ability. The upcoming MATLAB simulations will serve as critical evidence of the theoretical framework's validity, showcasing its performance under realistic operating conditions.

4. Simulation Results

This section presents the outcomes derived from implementing the proposed Reset Adaptive Super Twisting Sliding Mode Controller (RASTSMC) on a PEM fuel cell stack system equipped with a boost converter. The efficiency of control methods is evaluated through two main approaches: practical implementation and computer-based simulation. In this study, simulations were performed in the MATLAB environment, and a comparison with a similar, validated control method was conducted to verify the effectiveness of the proposed control strategy. Importantly, the practical implementation of the proposed controller represents the next phase of the authors' ongoing research.

The simulation setup utilized a hardware platform with the following specifications: An Intel Core i7-10750H processor, 16GB DDR4 RAM, a 512GB SSD, and an NVIDIA GeForce RTX 2060 GPU with 6GB GDDR6 memory. For benchmarking, the Proportional-Integral Adaptive Sliding Mode Controller (PI-ASMC) method, referenced from [19], was chosen for comparison.

The parameters for the PEM fuel cell components, including the number of cells in the stack, the membrane cross-sectional area, the stack operating temperature, PEM cell pressure, boost converter specifications, and reference current, were all adopted from [19]. Additionally, the control parameters were configured as follows:

$$k_P = 0.5, k_I = 40, \kappa_{iReset} = 0.01, \lambda = 0.01, k_1 = 1, k_2 = 1 \quad (36)$$

These parameter values were carefully selected based on system dynamics and prior studies to ensure the effectiveness and robustness of the proposed control scheme under varying conditions.

For evaluating the controller's performance, the same load variation as described in [19] was applied as an uncertainty factor. The load variation, illustrated in figure 6, introduces dynamic changes that test the controller's ability to maintain system stability and performance.

The consideration of load variation as a test condition is essential for evaluating the robustness and adaptability of the control system. A robust controller should maintain optimal performance despite external disturbances and parameter changes.

Under the specified conditions, the optimal current value for extracting maximum power from the fuel cell is $i_L = 9.74A$. Despite disturbances and the dynamic instability of the boost converter, this current must be accurately tracked. The simulation results, demonstrating the controller's performance, are presented in figures 7 through 12. Specifically, figures 7, 8, and 9 depict the output voltage of the controller, the PEM fuel cell, and the fuel cell stack, respectively.

These results provide valuable insights into the controller's ability to stabilize the system, track the reference current, and handle the nonlinear and uncertain dynamics of the fuel cell and converter. Such performance metrics are critical for evaluating the proposed control strategy against existing methods.

The figures clearly illustrate that the output voltage behavior under both the RASTSMC and PI-ASMC controllers is quite similar, with some key differences. The range of output voltage under the RASTSMC controller is slightly larger compared to the PI-ASMC method, and the voltage changes under the proposed technique are marginally greater. However, the RASTSMC controller exhibits a shorter settling time, enabling the system to reach its steady-state more quickly while displaying more stable behavior overall. The shorter settling time and enhanced stability highlight the effectiveness of the RASTSMC technique, especially in applications where rapid response and stable operation are critical for maintaining system performance.

Figure 10 compares the tracking of i_L (load current) under the RASTSMC and PI-ASMC methods. With the planned RASTSMC technique, the load current reaches the optimal i_L value more quickly, with significantly reduced fluctuations, overshoot, and undershoot. In contrast, the PI-ASMC method demonstrates less favorable transient and steady-state behavior, struggling with higher deviations and slower response. The errors in i_L, evaluated using various error criteria shown in Table 2, further confirms the superior tracking capability of the RASTSMC technique.

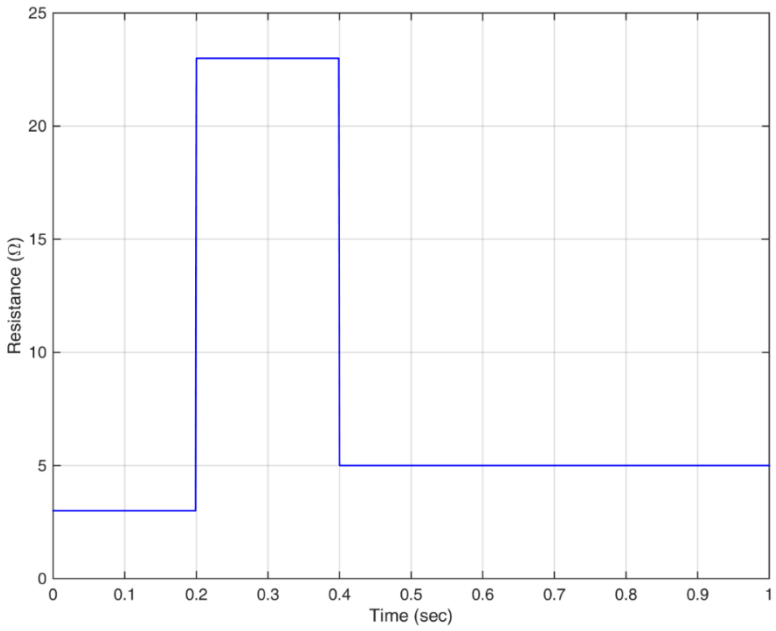

Figure 6. Considered Load variations in the simulation scenario

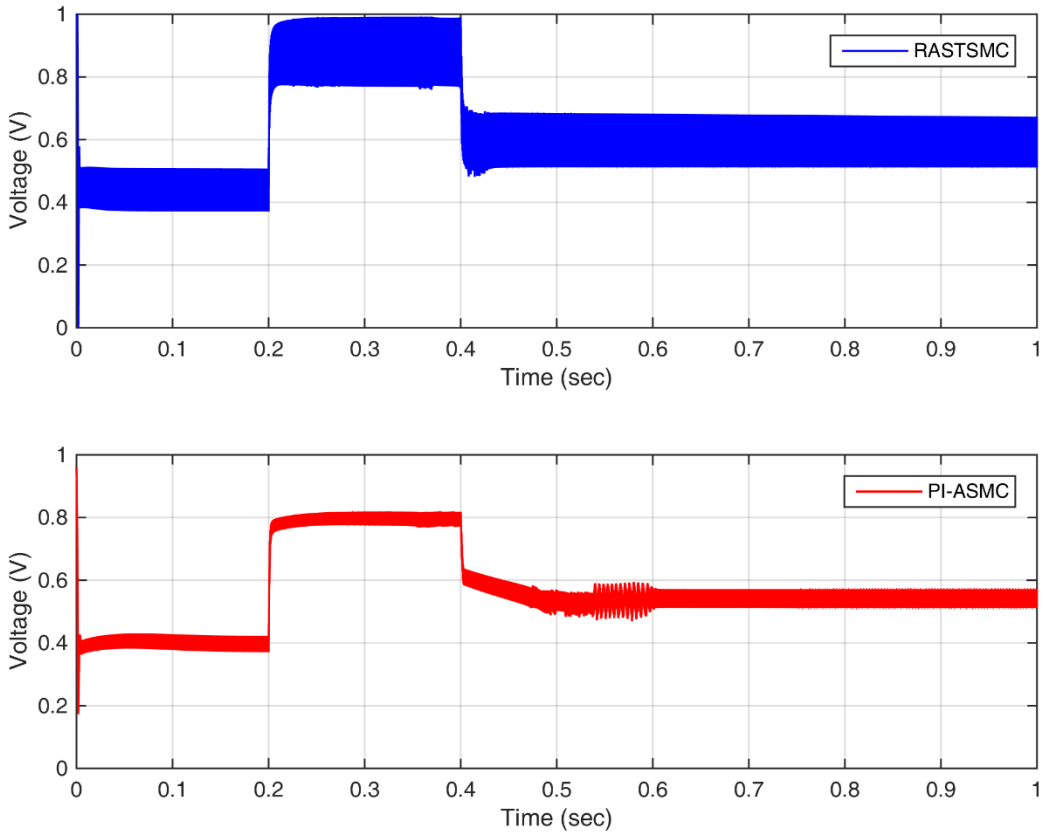

Figure 7. The output voltage of PI-ASMC and RASTSMC controllers

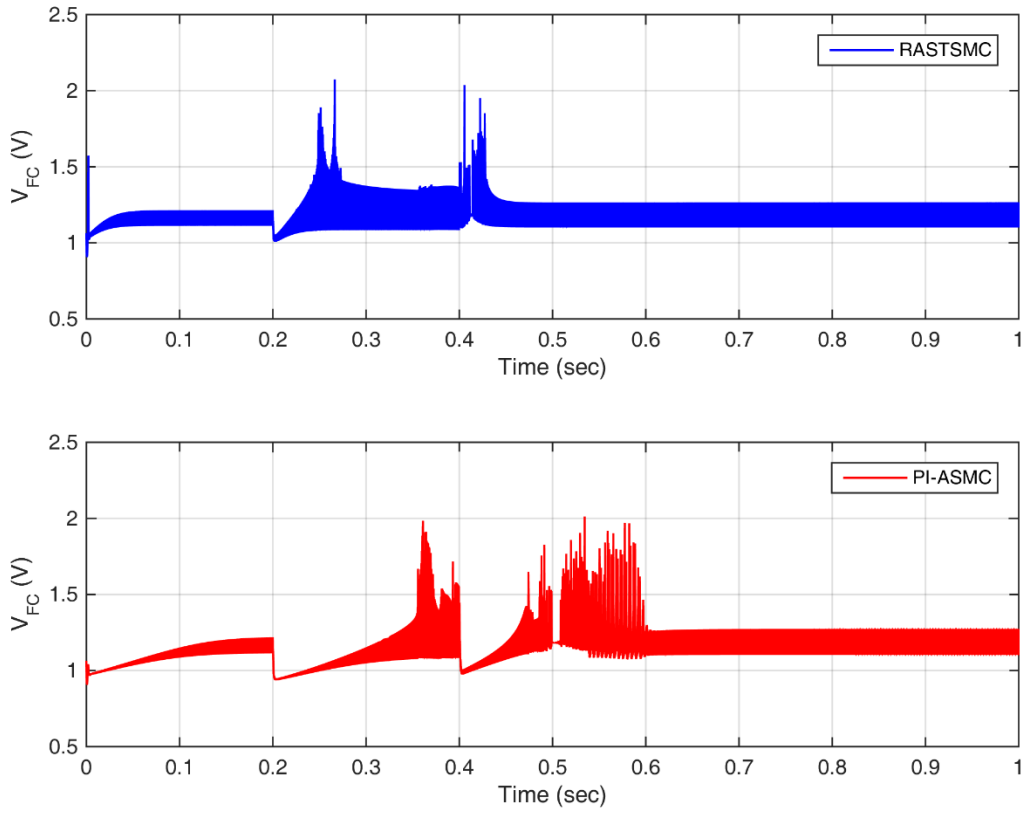

Figure 8. PEM fuel cell voltage under PI-ASMC and RASTSMC controllers

10.57647/spre.2026.1001.04

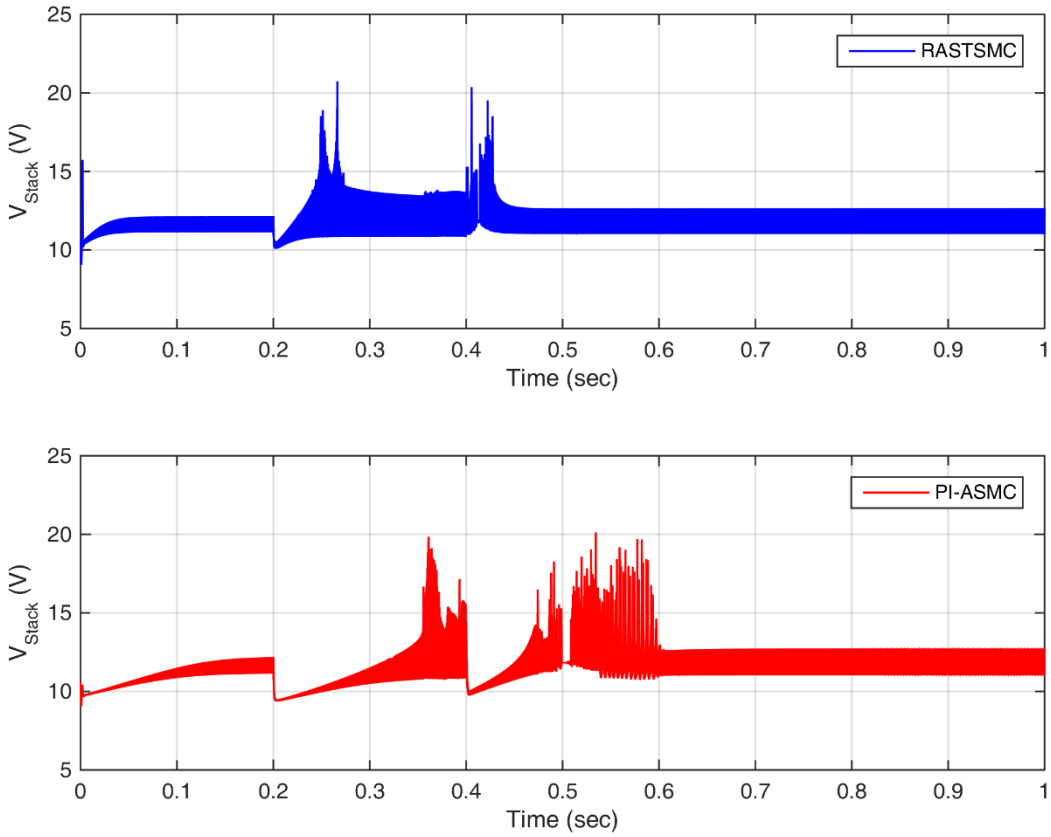

Figure 9. PEM fuel cell stack voltage under PI-ASMC and RASTSMC controllers

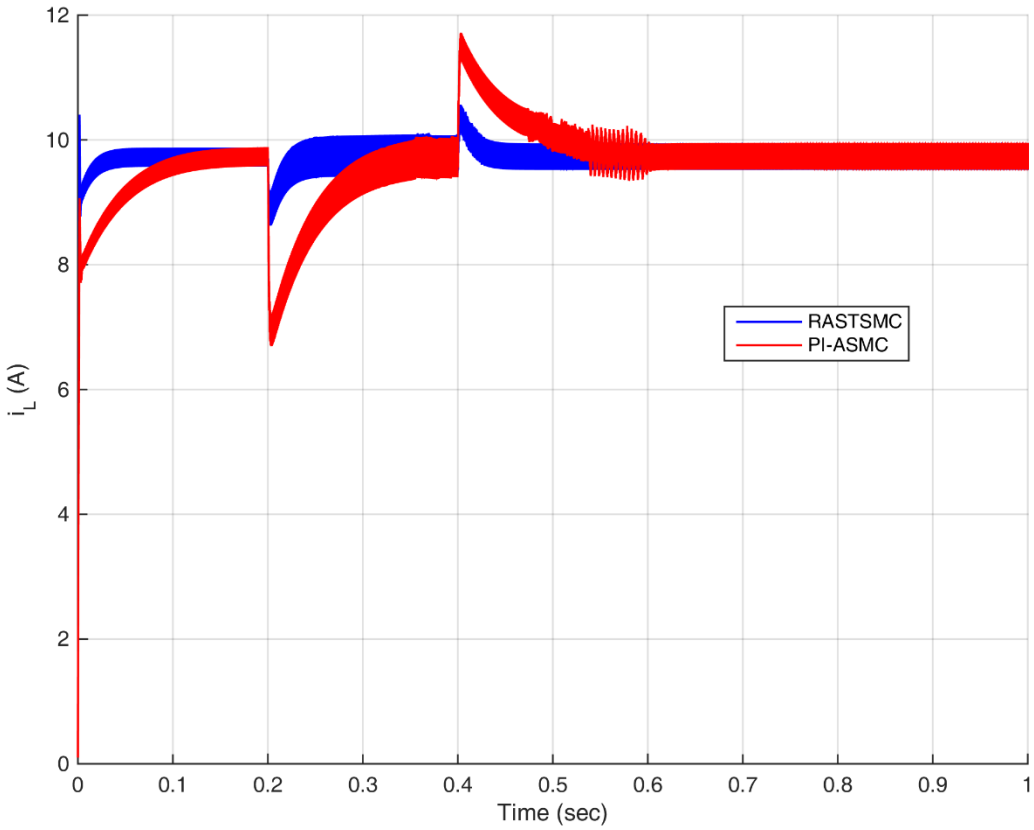

Figure 10. DC/DC boost converter output current under PI-ASMC and RASTSMC controllers

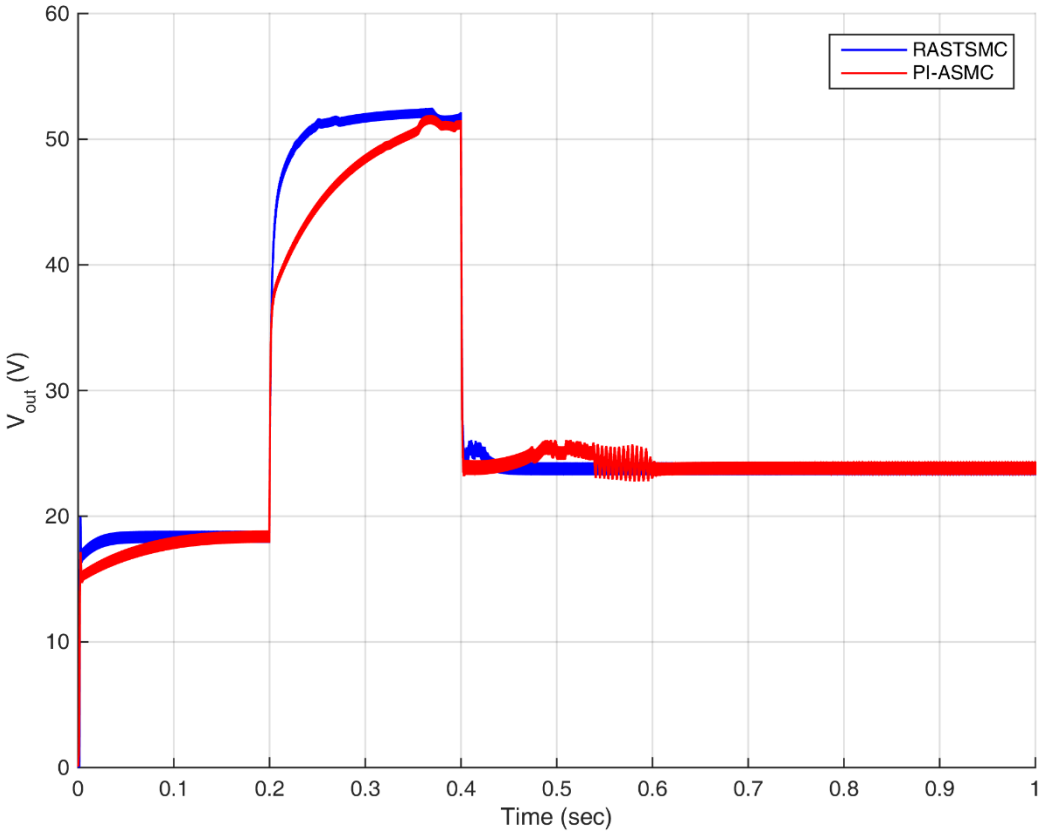

Figure 11. DC/DC boost converter output voltage under PI-ASMC and RASTSMC controllers

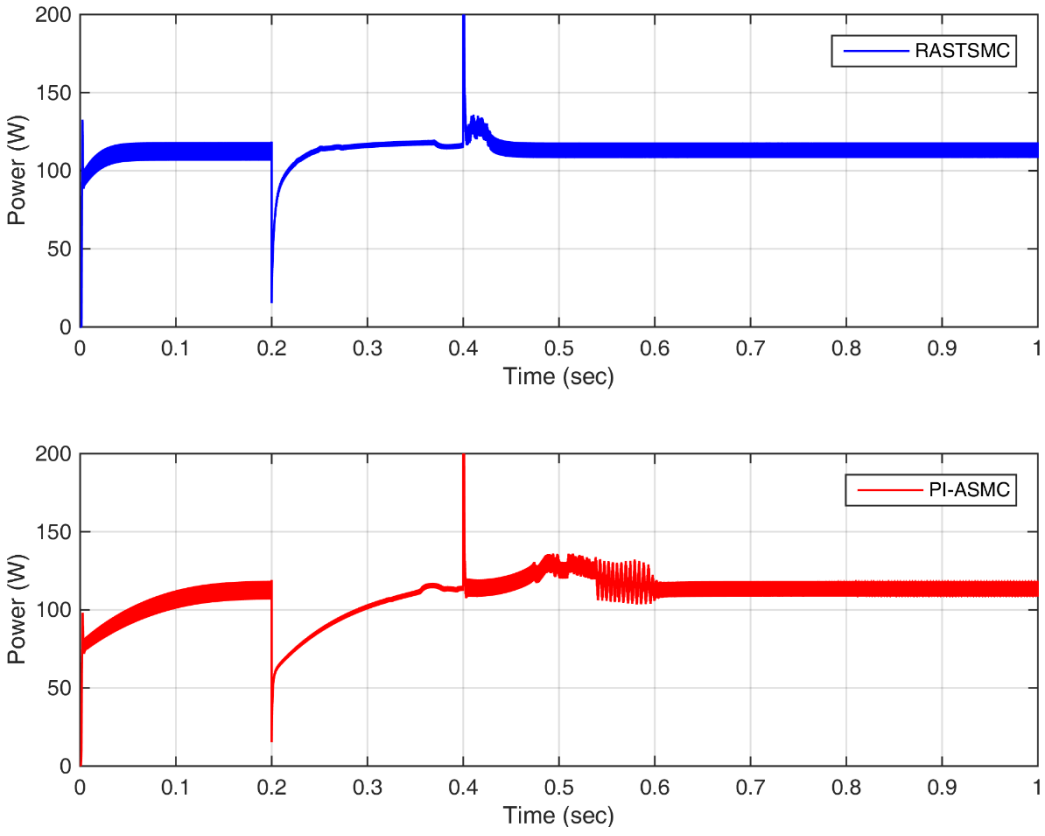

Figure 12. DC/DC boost converter output power under PI-ASMC and RASTSMC controllers

Table 2. Specifications of the i_L error value and overshoot

Controller	i_L					
	ISE	ITSE	IAE	ITAE	RMSE	Overshoot
PI-ASMC	0.4565	0.1083	0.4245	0.1567	0.7063	20.3050%
RASTSMC	0.0852	0.0148	0.1402	0.0606	0.2444	8.5046%

The ability to minimize fluctuations, overshoot, and tracking error is particularly important in fuel cell systems to ensure efficient energy extraction and prevent unnecessary stress on system components.

The output voltage of the DC/DC boost converter under the RASTSMC and PI-ASMC methods is presented in figure 11. The RASTSMC technique offers clear advantages, such as reduced settling time, higher response speed, and fewer fluctuations, demonstrating its superior performance in regulating the boost converter's output voltage.

These improvements in voltage regulation ensure stable operation of the fuel cell system, especially under varying load conditions and external disturbances, which are common in practical scenarios.

Finally, figure 12 depicts the output power from the fuel cell equipped with the boost converter. The advantages observed in the earlier results—such as reduced settling time, faster response, fewer fluctuations, and lower tracking error—are also evident here. The RASTSMC technique achieves optimal power extraction while maintaining system stability despite the non-minimum phase behavior of the boost converter, environmental uncertainties, and external disturbances.

Efficient power extraction and stable operation under dynamic conditions are critical for renewable energy systems, and the proposed controller demonstrates its capability to meet these demands effectively.

5. Conclusion

This study introduced a novel hybrid robust control scheme, combining reset and adaptive sliding mode techniques, to maximize power extraction from a PEM fuel cell system. The proposed RASTSMC method not only optimally adjusted the output voltage and load current but also significantly improved the transient and steady-state dynamics in terms of settling time, overshoot, undershoot, tracking speed, and tracking error. These improvements were achieved despite the presence of uncertainties, disturbances, and load variations. By effectively handling uncertainties and disturbances, the RASTSMC controller enhances the reliability and robustness of the fuel cell system, making it more suitable for real-world applications. The comparison with the PI-ASMC method demonstrated that the RASTSMC approach achieved more stable output power and voltage with fewer fluctuations, further validating its superiority. For future work, the practical implementation of the robust controller on the studied structure can be explored. Additionally, designing high-power fuel cell stacks using advanced manufacturing techniques, such as additive manufacturing, and incorporating predictive control methods to account for control signal limitations are promising directions for further research.

Authors Contribution
All authors have contributed equally to prepare the paper.

Availability of data and materials
Data available on request from the authors.

Conflict of interests
The authors declare that they have no known competing financial interests or personal relationships that could have appeared to influence the work reported in this paper.

References

[1] Behera, U. S., Sangwai, J. S., & Byun, H. S. (2025). A comprehensive review on the recent advances in applications of nanofluids for effective utilization of renewable energy. *Renewable and Sustainable Energy Reviews*, *207*, 114901.

[2] Tackie-Otoo, B. N., Mahmoud, M., & Raza, A. (2025). Renewable energy versus hydrogen energy: assessing current needs for sustainable energy solutions. *Energy & Fuels*, *39*(37), 17730-17762.

[3] Islam, A., Shahriar, M., Islam, M. T., Islam, T., Papia, A., Mohanta, S. C., ... & Awual, M. R. (2025). Recent breakthroughs and future horizons in next-generation HT-PEMs for hydrogen fuel cell. *International Journal of Hydrogen Energy*, *168*, 151113.

[4] Kiani, M., Zhao, Y., & Zhang, R. (2025). Proton exchange membrane fuel cells: recent developments and future perspectives. *Chemical Communications*, *61*(52), 9392-9411.

[5] Qasem, N. A., & Abdulrahman, G. A. (2024). A recent comprehensive review of fuel cells: history, types, and applications. *International Journal of Energy Research*, *2024*(1), 7271748.

[6] Omar, F. A. (2023). Comprehensive Analysis and Evaluation of DC-DC Converters: Advancements, Applications, and Challenges. *Black Sea Journal of Engineering and Science*, *6*(4), 557-571.

[7] Fan, S., & Xu, S. (2026). Optimal fuel cell control modeling with feedback linearization and adaptive sliding mode control. *Scientific Reports*.

[8] Kart, S., Demir, F., Kocaarslan, İ., & Genc, N. (2023). Increasing PEM fuel cell performance via fuzzy-logic controlled cascaded DC-DC boost converter. International Journal of Hydrogen Energy.

[9] Kabache, S., Reguieg, D., Bousbiat, E., & Kendil, D. (2025). Incremental fuzzy with PSO optimization for improving the pressure stability of hydrogen and oxygen recovery 5 kW PEM fuel cell system under variable load conditions. *International Journal of Hydrogen Energy*, *120*, 54-66.

[10] Ma, R., Wu, Y., Breaz, E., Huangfu, Y., Briois, P., & Gao, F. (2018, September). High-order sliding mode control of DC-DC converter for PEM fuel cell applications. In 2018, IEEE Industry Applications Society Annual Meeting (IAS) (pp. 1-7). IEEE.

[11] Silaa, M. Y., Barambones, O., Uralde, J., & Bencherif, A. (2025). Simulation and experimental validation of novel sliding mode control with quick power reaching law for a proton exchange membrane fuel cell system. *Journal of Power Sources*, *653*, 237632.

[12] Akter, F., Roy, T. K., Islam, M. S., Alkhateeb, A. F., & Mollah, M. A. (2022). Design of a nonlinear integral terminal sliding mode controller for a pem fuel cell based on a dc-dc boost converter. IEEE Access, 10, 97419-97428.

[13] Trinh, H. A., & Ahn, K. K. (2025). Adaptive disturbance observer-based terminal sliding mode algorithm for a Mini excavator proton exchange membrane fuel cell air feeding system. *Applied Energy*, *382*, 125304.

[14] Chen, Yiyu, Mengjun Long, Sai Jiang, Yuanli Liu, Zizhang Zhan, Lihua Wang, and Zhongmin Wan. "Feedback linearized sliding mode controller for high-power PEMFC thermal management system adapted to road driving cycle." *Energy Conversion and Management: X* (2025): 101189.

[15] İnci, M., & Özbek, N. S. (2025). A novel predictive current sliding mode control for improving the performance efficiency of fuel cell vehicle-to-load (V2L) system with boost converter. *International Journal of Hydrogen Energy*, *138*, 973-984.

[16] Tan, S. C., Lai, Y. M., Tse, C. K., & Cheung, M. K. (2006). Adaptive feedforward and feedback control schemes for sliding mode controlled power converters. IEEE Transactions on Power Electronics, 21(1), 182-192.

[17] Cid-Pastor, A., Martinez-Salamero, L., El Aroudi, A., Giral, R., Calvente, J., & Leyva, R. (2013). Synthesis of loss-free resistors based on sliding-mode control and its applications in power processing. Control Engineering Practice, 21(5), 689-699.

[18] López-Lapeña, O., Penella, M. T., & Gasulla, M. (2009). A new MPPT method for low-power solar energy harvesting. IEEE Transactions on Industrial Electronics, 57(9), 3129-3138.

[19] Gao, J., Yang, Y., & Gu, H. (2021). Improving the output power of PEM fuel cell with PI+ ASM combined controller designed for boost converter. Journal of New Materials for Electrochemical Systems, 24(4).

[20] Uzunoglu, M., & Alam, M. S. (2006). Dynamic modeling, design, and simulation of a combined PEM fuel cell and ultracapacitor system for stand-alone residential applications. IEEE transactions on energy conversion, 21(3), 767-775.

[21] Wang, C., Nehrir, M. H., & Shaw, S. R. (2005). Dynamic models and model validation for PEM fuel cells using electrical circuits. IEEE transactions on energy conversion, 20(2), 442-451.

[22] Yigit, T., & Selamet, O. F. (2016). Mathematical modeling and dynamic Simulink simulation of high-pressure PEM electrolyzer system. International Journal of Hydrogen Energy, 41(32), 13901-13914.